NANO LETTERS

Letter

pubs.acs.org/NanoLett

Rapid Sequential in Situ Multiplexing with DNA Exchange Imaging in Neuronal Cells and Tissues

Yu Wang,[†,‡,§,□] Johannes B. Woehrstein,[†,‡] Noah Donoghue,[†,§,△] Mingjie Dai,[†,‡,■] Maier S. Avendaño,[†,‡] Ron C. J. Schackmann,[∥] Jason J. Zoeller,[∥] Shan Shan H. Wang,[⊥,○] Paul W. Tillberg,[▽,¶,●] Demian Park,[▽] Sylvain W. Lapan,[§] Edward S. Boyden,[#,▽] Joan S. Brugge,[∥] Pascal S. Kaeser,[⊥] George M. Church,[†,§] Sarit S. Agasti,[*,†,‡] Ralf Jungmann,[*,†,‡] and Peng Yin[*,†,‡]

[†]Wyss Institute for Biologically Inspired Engineering, [■]Program in Biophysics, Harvard University, Boston, Massachusetts 02115, United States

[‡]Department of Systems Biology, [§]Department of Genetics, [∥]Department of Cell Biology, [⊥]Department of Neurobiology, [□]Program in Biological and Biomedical Sciences, [○]Program in Neuroscience, Harvard Medical School, Boston, Massachusetts 02115, United States

[#]Department of Biological Engineering, [▽]Media Lab, [¶]Department of Brain and Cognitive Sciences, [●]Department of Electrical Engineering and Computer Science, Massachusetts Institute of Technology (MIT), Cambridge, Massachusetts 02139, United States

[△]Warren Alpert Medical School, Brown University, Providence, Rhode Island 02903, United States

Supporting Information

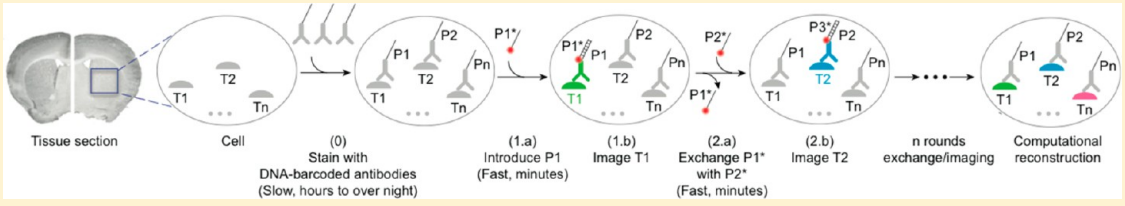

ABSTRACT: To decipher the molecular mechanisms of biological function, it is critical to map the molecular composition of individual cells or even more importantly tissue samples in the context of their biological environment in situ. Immunofluorescence (IF) provides specific labeling for molecular profiling. However, conventional IF methods have finite multiplexing capabilities due to spectral overlap of the fluorophores. Various sequential imaging methods have been developed to circumvent this spectral limit but are not widely adopted due to the common limitation of requiring multirounds of slow (typically over 2 h at room temperature to overnight at 4 °C in practice) immunostaining. We present here a practical and robust method, which we call DNA Exchange Imaging (DEI), for rapid in situ spectrally unlimited multiplexing. This technique overcomes speed restrictions by allowing for single-round immunostaining with DNA-barcoded antibodies, followed by rapid (less than 10 min) buffer exchange of fluorophore-bearing DNA imager strands. The programmability of DEI allows us to apply it to diverse microscopy platforms (with Exchange Confocal, Exchange-SIM, Exchange-STED, and Exchange-PAINT demonstrated here) at multiple desired resolution scales (from ~300 nm down to sub-20 nm). We optimized and validated the use of DEI in complex biological samples, including primary neuron cultures and tissue sections. These results collectively suggest DNA exchange as a versatile, practical platform for rapid, highly multiplexed in situ imaging, potentially enabling new applications ranging from basic science, to drug discovery, and to clinical pathology.

KEYWORDS: *Highly multiplexed imaging, super-resolution imaging, in situ protein detection, multiplexed cell type identification, in situ protein−protein colocalization analysis*

Fluorescence microscopy has become a standard tool to characterize specimens in biological and biomedical studies. One of its advantages is the widespread availability of protein-specific labeling reagents such as antibodies. However, while dye-labeled antibodies allow for easy target labeling, the spectral overlap of multiple fluorophores leads to limited multiplexing capabilities (e.g., typically no more than four targets). This shortcoming currently prevents studies targeted toward investigating network-wide changes in single cells and tissues using fluorescence microscopy. Various techniques, including "dye-cycling" by repeated antibody staining,[1−8] multiplexed ion beam imaging (MIBI),[9−11] spectrally resolved stochastic reconstruction microscopy (SR-STORM),[12] as well as others,[13−16] have been developed to overcome current limitations for multitarget detection, enabling highly multiplexed imaging studies (see Table S1 for a detailed comparison

Received: June 27, 2017
Revised: September 19, 2017
Published: September 21, 2017

DOI: 10.1021/acs.nanolett.7b02716
Nano Lett. 2017, 17, 6131−6139

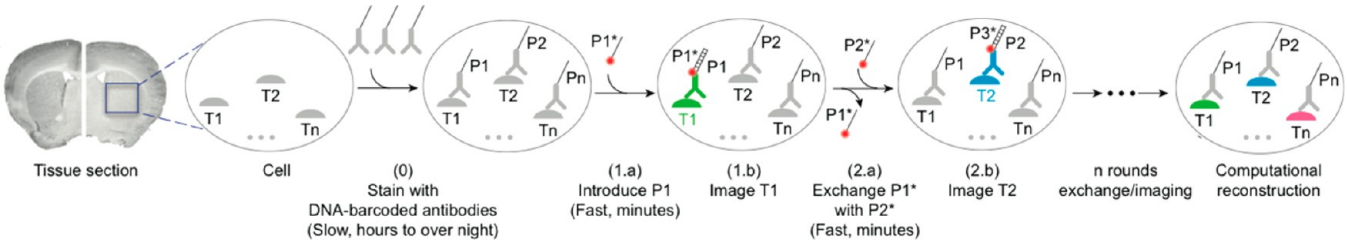

Figure 1. DNA Exchange Imaging. Distinct targets (T1, T2, ..., T*n*) are labeled using corresponding antibodies conjugated to orthogonal DNA docking strands (P1, P2, ..., P*n*) in a single step. Imager strands (P1*, P2*, ..., P*n**) are sequentially introduced to visualize target signals. The imager strands are washed away rapidly using low ionic strength buffer after each round of imaging. After imaging, all images are computationally registered, and a final merged image is reconstructed by assigning pseudocolors to each target image.

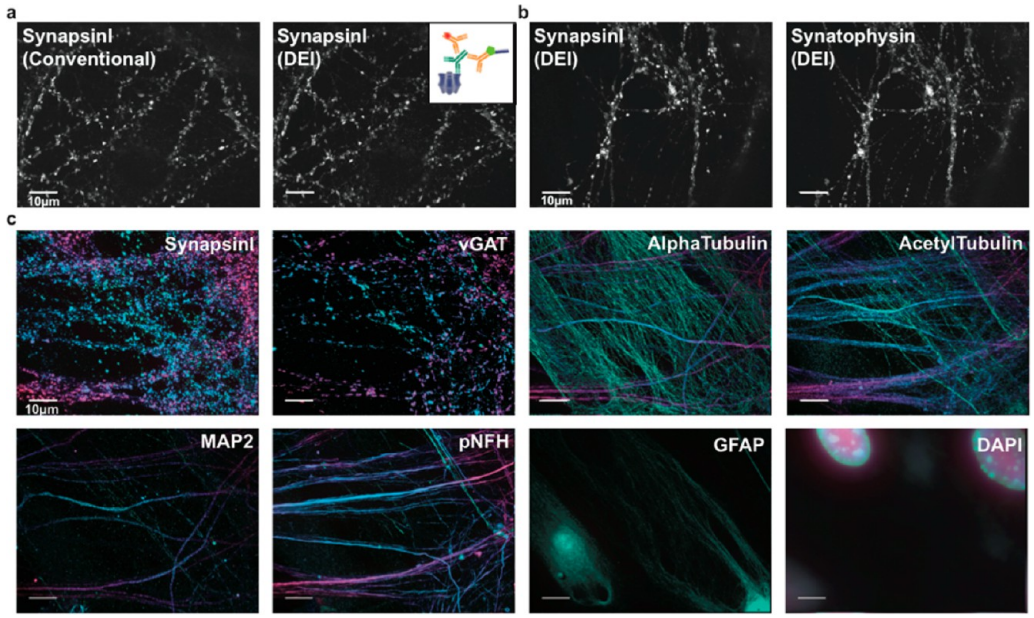

Figure 2. Multiplexed diffraction-limited confocal imaging with DEI. (a) Comparison of conventional staining using dye-conjugated antibodies and DEI using DNA-conjugated antibodies. Fixed neurons were stained with primary antibodies targeting SynapsinI, followed by both Alexa647-conjugated and DNA-conjugated antibodies, as shown in the schematic. DNA-conjugated antibody signals were visualized using Cy3b-imager strands. The correlation coefficient of the two images was 0.96. (b) Co-localization of SynapsinI and Synaptophysin in neurons visualized using two rounds of DEI. (c) Multiplexed eight-target imaging in neurons. Fixed DIV (days in vitro) 14 mouse hippocampal neurons were stained with DNA-conjugated antibodies against SynapsinI, vGAT, MAP2, pNFH, GFAP, AlphaTubulin, and AcetylTubulin. A 3D image stack of 14 μm thickness in *z*-axis was taken for each target and displayed as 2D color-coded maximum intensity projection (bottom to top: green to red). Scale bars: 10 μm. DNA docking strand sequences are listed in Table S4.

of these different techniques). However, these techniques have thus far not been broadly adopted due to practical limitations: they are typically time-intensive (e.g., due to repeated antibody staining as in current dye-cycling techniques, with each round of staining taking hours at room temperature and preferentially overnight at 4 °C for optimal labeling), and/or they are difficult to be directly implemented into current widely available microscope systems because specialized instruments are often required (e.g., as MIBI and SR-STORM).

To overcome current limitations, we introduce DNA Exchange Imaging (DEI), a generalization of our previously developed Exchange-PAINT[17] technique, providing a fast and practical method to perform highly multiplexed fluorescence imaging using standard, commercially available microscopy platforms. We have previously demonstrated DEI in the form of Exchange-PAINT.[17] In this paper, we show that the DEI principle can be generalized to other super-resolution microscopy systems, including SIM and STED, with new DNA sequence design and imaging setting. More importantly, with an optimized design, we extend DEI to standard resolution confocal microscopes that are widely available in common biological laboratories. Unlike the fluorescence "blinking" in our previous single molecule-based Exchange-PAINT, we use pseudopermanent and dense target labeling with fluorophore-conjugated complementary imager strands, thus permitting rapid image acquisition (typically <1 s exposure time) and deeper sample penetration (tens of micrometers versus a few hundred nanometers in PAINT) while maintaining the fast imager removal capability by simple and gentle buffer exchange. This unique advantage of our new protocol enables us to perform in situ multiplexing in more complex biological systems such as primary neuron cultures and biological tissue samples (as compared to thin layer of cells in our previous[17] and recent[18] super-resolution Exchange-PAINT work).

In DEI, we employ DNA-barcoded antibodies—instead of dye-labeled antibodies—that are conjugated with short DNA oligos (typically 9–10 nucleotides long for implementations in this paper) called docking strands.[17−19] Multiplexed protein

DOI: 10.1021/acs.nanolett.7b02716
Nano Lett. 2017, 17, 6131−6139

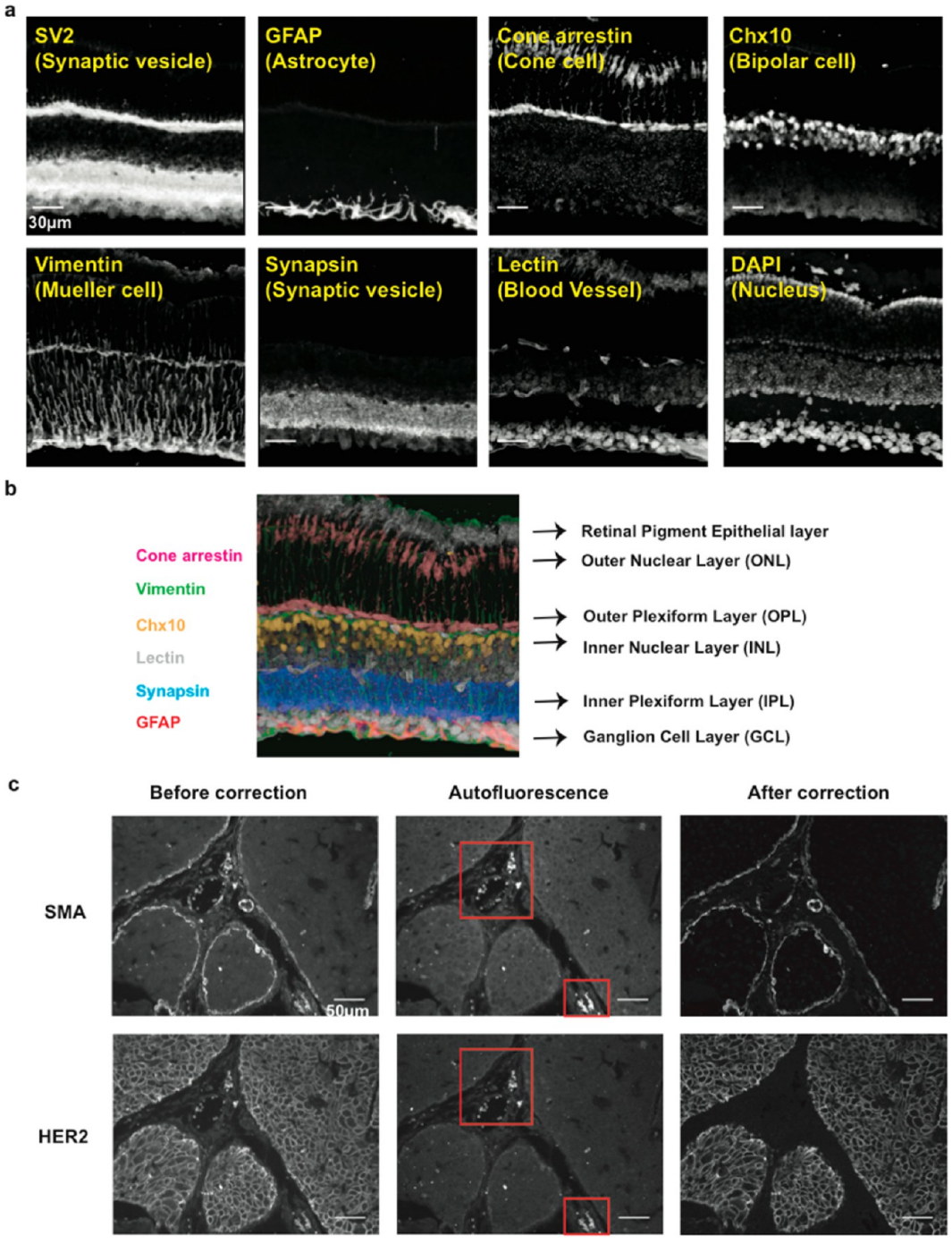

Figure 3. Multiplexed DEI of tissue samples. (a) A 40 μm thick fresh frozen mouse retina section was stained with antibodies targeting SV2, GFAP, Cone arrestin, Chx10, Vimentin, and Synapsin. 3D images were taken with six rounds of exchange of Cy3b-labeled imager strands. Blood vessels were stained with Alexa488-conjugated lectin probes and imaged in every exchange cycle for image registration. The nucleus was stained with DAPI. Scale bars: 30 μm. (b) Merged six-target image reveals different layers of cells in the retina. (c) Autofluorescence correction with DEI on a paraffin-embedded breast tumor section. Autofluorescence images were taken before adding imager strands with the same laser intensity and camera exposure time and then subtracted from the corresponding target images to obtain autofluorescence-corrected images. Note that the strong autofluorescence (presumably from blood cells, labeled with red square) was eliminated in the corrected images. Scale bars: 50 μm. DNA docking strand sequences are listed in Tables S5 and S7.

target labeling is performed efficiently by single-step simultaneous immunostaining with antibodies carrying orthogonal DNA docking strands, followed by image acquisition where dye-labeled complementary imager strands are applied sequentially via rapid buffer exchange (Figure 1). We demonstrated 8-target imaging in primary neuron cultures and in tens of micro thick retina tissue sections in 2−3 h (as compared to days required in principle by previous methods using comparable equipment) to visualize distinct cellular structures and to annotate different cell types. In addition to providing a rapid and simple multiplexed imaging method, Exchange Confocal, as well as other DEI methods, enables easy autofluorescence correction, and is naturally chromatic aberration-free and photobleaching-resistant (Figure S1).

DOI: 10.1021/acs.nanolett.7b02716
Nano Lett. 2017, 17, 6131−6139

Exchange-PAINT[17] has been previously developed to perform multiplexed single-molecule localization-based SR imaging. Despite its superior resolution, its utility is restricted due to its imaging time and depth trade-off. It requires recording a time-lapse movie of single molecule blinking events for final SR image reconstruction, which typically takes minutes to even hours for a single reconstructed image. In addition, the high signal-to-noise ratio requirement for PAINT imaging, single-molecule-compatible microscopes (usually total internal reflection fluorescence microscopes) are necessary, limiting the imaging depth to typically a few hundred nanometers above the coverslip. Moreover, diffraction-limited imaging is often sufficient for experiments that only require single-cell resolution (e.g., pathological analysis). In SR PAINT imaging, sparse labeling of targets with transiently binding imager strands is required for single-molecule localization. In contrast, diffraction-limited Exchange-Confocal imaging shown here aims to capture signals from all of the molecules of a certain target in a single image frame, which requires pseudopermanent and dense target labeling with imager strands. To achieve this, we tuned three parameters: imager/docking strand association time, imager strand concentration, and camera exposure time. First, we designed imager/docking strand duplexes with higher binding affinity to attain a relatively slow dissociation rate (0.2 s^{-1} for a 10 base-pair duplex on average[19]) by increasing the length of the DNA duplex (Figure S2). To minimize the number of unoccupied docking sites, we used a high concentration of imager strand (e.g., 10 nM as compared to 1 nM in single-molecule PAINT applications) to densely label the docking sites for the corresponding target (Figure S2). Furthermore, we used longer camera exposure times (typically 50−300 ms for a widefield microscope and 500 ms to 5 s for a spinning disk confocal microscope) to minimize unoccupied docking sites and enhance the signal-to-noise ratio.

As a result, we achieved diffraction-limited Exchange-Confocal imaging with a quality comparable to that of conventional IF methods. To examine signal specificity of Exchange-Confocal, we compared the Exchange-Confocal images with those attained by conventional IF methods using fluorophore-conjugated antibodies (Figure 2a and Figure S3). We labeled synapses with the marker protein SynapsinI using primary antibodies followed by secondary antibodies conjugated either with DNA docking strands or with Alexa488 dye. The SynapsinI signals from Exchange-Confocal and from conventional IF were obtained with 561 nm and with 488 nm excitation, respectively. We observed colocalization of fluorescence signals from these two methods with a correlation coefficient of 0.96. We also performed Exchange-Confocal based colocalization analysis of SynapsinI and Synaptophysin, both of which are present in synaptic vesicles (Figure 2b). We obtained a correlation coefficient of 0.80, which is similar to values that have been reported using array tomography.[20]

As Exchange-Confocal requires sequential application of imager strands labeled with the same fluorophore, the efficient imager strand removal is critical. We tested changes in fluorescence intensity between each cycle of imager strand exchange (Figure S4). DIV14 mouse hippocampal neurons were fixed and stained with antibodies against glial fibrillary acidic protein (GFAP, a marker protein for astrocytes) and beta3Tubulin (a marker protein for neurons). P1* and P2* imager strands were sequentially applied to visualize GFAP and beta3Tubulin, respectively. The fluorescence intensity after washing with PBS decreased to the background level and thus was negligible compared to signal levels in the other images, confirming the sufficiently efficient removal of imager strands from the solution.

To demonstrate multiplexed Exchange-Confocal, we next imaged eight targets in a fixed primary mouse hippocampal neuron culture (Figure 2c and Movie 1). SynapsinI antibodies were used to mark all synapses, and vesicular GABA transporter (vGAT) antibodies labeled inhibitory synapses. Five other structural proteins were also labeled, including microtubule associated protein 2 (MAP2) (a dendritic marker), phosphorylated neurofilament heavy chain (pNFH) (in neurites), AlphaTubulin (microtubule component), AcetylTubulin (microtubule component), and GFAP (an astrocyte marker). DAPI was used to stain nuclei. For the eight protein targets, we performed dual-color imaging (using Cy3b- and Atto655-conjugated imager strands) to reduce probe exchange cycles. The sample drift was monitored by signals from the 488 nm channel, and images were registered accordingly (Figure S5).

Three-dimensional (3D) images were taken for each target using a spinning disk confocal microscope, and the color-coded 2D maximum projection images were displayed for each target (Figure 2c). We used green and red colors to represent the signals from the bottom and top focal planes, respectively. A color gradient from green to red was used to represent the signals from intermediate focal planes. Astrocytes, labeled with GFAP, were mostly shown in green, consistent with the fact that astrocytes grew beneath neurons. SynapsinI labeled both excitatory and inhibitory synapses, while vGAT only labeled inhibitory synapses. As expected, SynapsinI signals were more abundant than those of vGAT. AlphaTubulin was observed in both astrocytes and neurons across the whole z-stack, and acetylTubulin was highly expressed in neurons.

To test the applicability of Exchange-Confocal to tissue samples, we performed eight-target Exchange-Confocal in fresh-frozen mouse retina tissue sections (Figure 3a and b). We chose retina samples because the tissue organization has been intensively studied and different cell types can be distinguished using protein markers.[21,22] A 40 μm thick retina section was stained using DNA-conjugated antibodies against SV2, GFAP, Cone arrestin, Chx10, Vimentin, and Synapsin and imaged with six rounds of exchange using Cy3b-conjugated imager strands. Lectin-Alexa488 was used to stain blood vessels and imaged for every exchange cycle for image registration. DAPI was used to stain the nucleus. As expected, every protein species was truthfully detected using Exchange-Confocal with the distribution of each target being in line with previous reports.[21−23] SV2 and Synapsin are both located in synapses. SV2 exists in both outer plexiform layer (OPL) and inner plexiform layer (IPL), whereas Synapsin is only located in the IPL, similar to what has been reported in salamander retina[24] (Figure 3b). It should be noted that SynapsinI antibody was used to stain the sample and the lack of Synapsin signal in the OPL only reflects the absence of SynapsionI, which could be replaced by alternative forms of Synapsin, such as Synapsin II or III. GFAP marks astrocytes that are located close to the ganglion cell layer (GCL) and Muller glial endfeet. Cone arrestin marks the cone photoreceptor cells in the outer nuclear layer (ONL). Vimentin labels Muller cells that spread across multiple layers. Chx10 is a pan-bipolar cell marker[23] located in the inner nuclear layer (INL). Another five-target Exchange-Confocal experiment was performed on a 10 μm thick formaldehyde fixed mouse brain section (Figure S6).

DOI: 10.1021/acs.nanolett.7b02716
Nano Lett. 2017, 17, 6131−6139

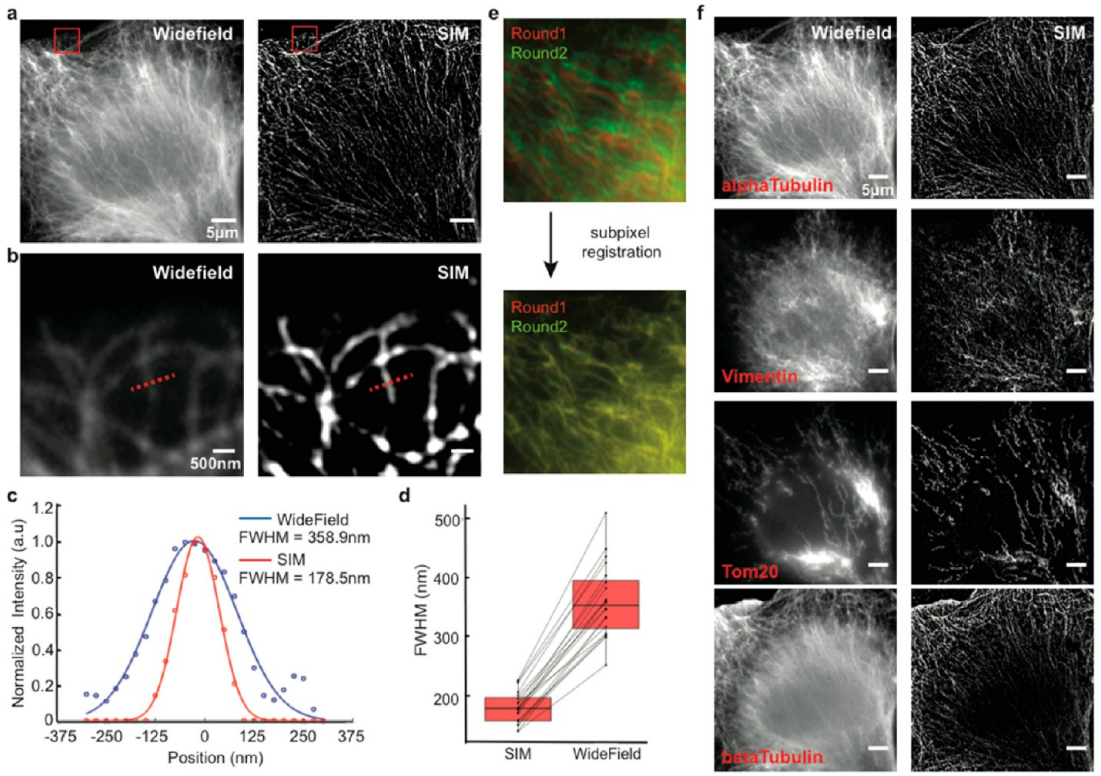

Figure 4. Four-target DEI with SIM in BSC1 cells. (a) Comparison of wide-field and SIM images on alphaTubulin. Scale bars: 5 μm. (b) Zoom-in views of the microtubules highlighted by red square in panel a. (c) Measurement of the apparent width of microtubules using a full-width at half-maximum (fwhm) criterion. The intensity plot of the cross-section highlighted in panel b was fitted using a Gaussian. (d) fwhm measurement of 20 microtubule cross sections revealed 2.014 ± 0.045 fold reduction of fwhm (the error range is SEM; boxes denote median values ± quartiles). (e) Subpixel registration of images in different exchange rounds. Vimentin was stained with both DNA-conjugated and Alexa488-labeled antibodies, and the 488 nm channel used for image registration. (f) Multiplexed 3D Exchange-SIM imaging in BSC1 cells. The 2D maximum intensity projections are presented here. Scale bars: 5 μm. DNA docking strand sequences are listed in Table S8.

We also tested Exchange-Confocal in paraffin-embedded tissue samples and performed two rounds of probe exchange to visualize HER2 and smooth muscle actin (SMA) in a 4 μm formalin-fixed and paraffin-embedded intraductal breast tumor carcinoma tissue from a HER2+ xenograft of SUM225 tumor cells[25] (Figure 3c). SMA stains the myoepithelial cells surrounding the intraductal tumor as well as stromal fibroblasts. We also note that Exchange-Confocal permits simple autofluorescence correction, an additional advantage over conventional fluorescence imaging for tissue samples. Autofluorescence, caused by the presence of various endogenous molecules (e.g., reduced NAD(P)H, flavins, reticulin fibers, lipofuscins, elastin, and collagen), can mask true target signals.[26] Although a few approaches have been developed, such as autofluorescence quenching using Sudan Black B, photobleaching with high intensity lasers, and postmeasurement image correction using complex mathematical models, they require optimization specific for each type of sample and/or may cause sample damage if harsh treatment is performed.[26] When performing DEI—as fluorophore-tagged imager strands are not added until the sample is ready to be imaged on the microscope—an image exhibiting only autofluorescence can be acquired immediately before the addition of imager strands and subsequently subtracted from the true target image. In Figure 3c, autofluorescence signals were captured before the addition of imager strands in the same field of view. Compared with images before correction, the "false" signals indicated by the red arrows were significantly reduced in the corrected images. It should be noted that the laser intensity and camera exposure time for autofluorescence images should be identical to those used for the real target image to ensure accurate correction.

Although diffraction-limited Exchange-Confocal enables faster and deeper sample imaging, its resolution may not be sufficient to address certain biological questions that require subcellular resolution. To achieve this, we applied DNA-Exchange-Imaging to various fast SR imaging microscopy platforms. First, we performed DEI using structured illumination microscopy (SIM), which doubles the achievable resolution.[27] Here in Exchange-SIM, we stained BSC1 cells with antibodies against AlphaTubulin followed by DNA-conjugated secondary antibodies (Figure 4a and b). We measured the full width at half-maximum (fwhm) of microtubules by Gaussian fitting the intensity plot of 20 microtubule cross sections and obtained an average of ~2-fold reduction of fwhm, consistent with the theoretical resolution enhancement for commercial SIM microscopes (Figure 4c and d and Table S11). While improving spatial resolution helps to resolve fine molecular structures, it also renders the experiment more sensitive to sample drift during buffer exchange process. To reduce drift-induced errors, we adapted a phase correlation-based algorithm[28] to perform subpixel registration (see Methods for more details). The algorithm correctly identified sample drift between different exchange cycles and registered images accordingly (Figure 4e). Multiplexed SIM imaging was performed with four rounds of exchange with Cy3b-conjugated imager strands targeting alphaTubulin, Vimentin, Tom20, and

DOI: 10.1021/acs.nanolett.7b02716
Nano Lett. 2017, 17, 6131−6139

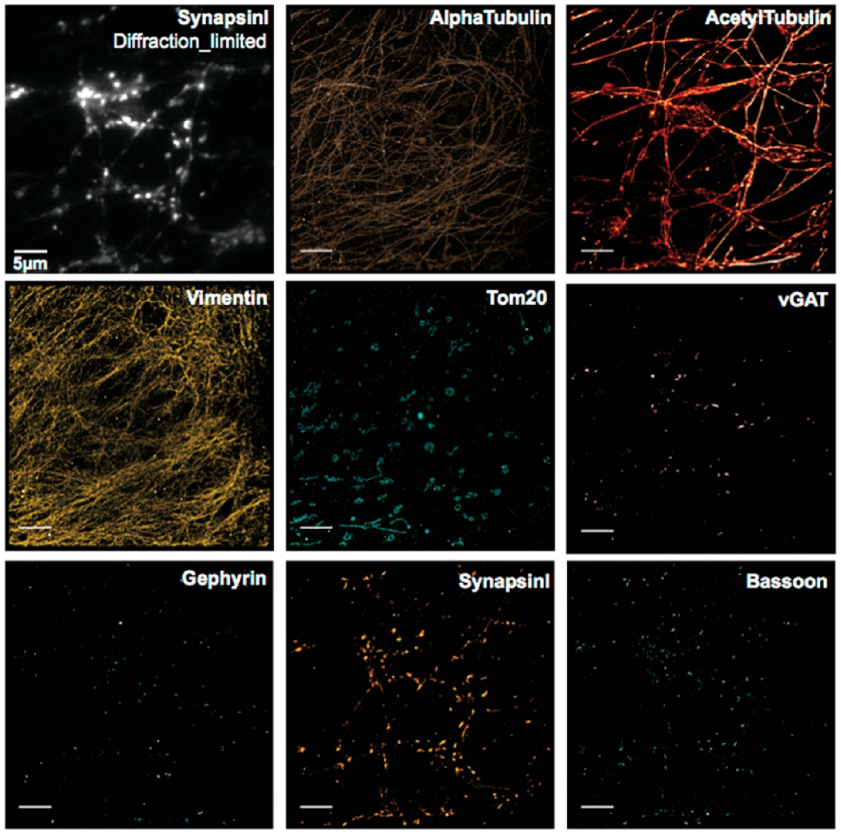

Figure 5. Eight-target chromatic aberration-free Exchange-PAINT imaging in primary neurons. Fixed DIV14 mouse hippocampal neurons were stained with DNA-conjugated antibodies targeting AlphaTubulin, Vimentin, vGAT, Gephyrin, SynapsinI, Bassoon, AcetylTubulin, and Tom20. SynapsinI was additionally labeled with Alex488-conjugated secondary antibodies for selecting regions of interest. In total, eight rounds of Exchange-PAINT imaging with Atto655-conjugated imager strands were performed to visualize all targets. Scale bar: 5 μm. DNA docking strand sequences are listed in Table S10.

betaTubulin (Figure 4f). An upsampling factor of 5 in the *x*- and *y*-axes and a factor of 2 in *z*-axis were used to perform subpixel image registration, resulting in a subpixel precision of 5 nm in the *x* and *y*-axes and 75 nm in the *z*-axis.

A similar multiplexed experiment was performed using a STED microscope (Figure S7). Together with previous related Exchange-STED work applied to synthetic DNA nanostructures,[29] our results show that DEI is generally compatible with SIM and STED microscopy and can be used for rapid multiplexed SR imaging.

For even higher spatial resolutions, we turned to our previous Exchange-PAINT[17] method and demonstrated eight-target super-resolution imaging in cultured neurons. DIV14 mouse hippocampal neurons were fixed and stained with antibodies against AcetylTubulin, AlphaTubulin, Vimentin, Tom20, SynapsinI, Bassoon, vGAT, and Gephyrin, utilizing our recently developed DNA-antibody labeling chemistry.[18] While synapsinI and vGAT antibodies label all and inhibitory synaptic vesicle clusters, respectively, Bassoon is a marker for the presynaptic active zone, and gephyrin marks postsynaptic scaffolds at inhibitory synapses. AcetylTubulin and AlphaTubulin are both microtubule components. Vimentin is a protein component in intermediate filaments, and Tom20 is located in the mitochondria. Eight rounds of Exchange-PAINT imaging with Atto655-conjugated imager strands were performed to visualize each target (Figure 5).

To demonstrate the improvement in resolution, we compared the quality of diffraction-limited and SR images for microtubules and merged Bassoon and Gephyrin from Figure 5 (Figures S8 and S9). Individual microtubule filaments were clearly resolved in the SR image but not in the diffraction-limited image (Figure S8a and b). A region was selected for a magnified view with two microtubules in close proximity to each other, and the distance between the two filaments was measured to be 108 nm (Figure S8c and d). In the Bassoon and Gephyrin merged image, presynaptic Bassoon signals can be distinguished from the postsynaptic Gephyrin signals in the SR image but not in the diffraction-limited image (Figure S9).

One unique application of multiplexed imaging is to detect protein−protein colocalization. To test the applicability of Exchange-PAINT for such studies, we merged the four synaptic protein images from Figure 5 to assay colocalization of these proteins (Figure 6a). We first compared the diffraction-limited and super-resolution images. Individual synapses are difficult to distinguish from each other in the diffraction-limited images but can be clearly visualized in the super-resolution images (Figure 6b). Particularly, the synapse orientation can be detected by lining synapsin (synaptic vesicle marker that is further from the presynaptic membrane), Bassoon (active zone marker that is closer to the presynaptic membrane) and gephryin (postsynaptic density marker on the postsynaptic sites) (Figure 6b). We also selected one region for a magnified view (Figure 6c). SynapsinI and Bassoon are known to be present in both excitatory synapses and inhibitory synapses, whereas vGAT and Gephyrin selectively label inhibitory synapses.[20] Three synapses were included in this region. Two of them contained only

DOI: 10.1021/acs.nanolett.7b02716
Nano Lett. 2017, 17, 6131−6139

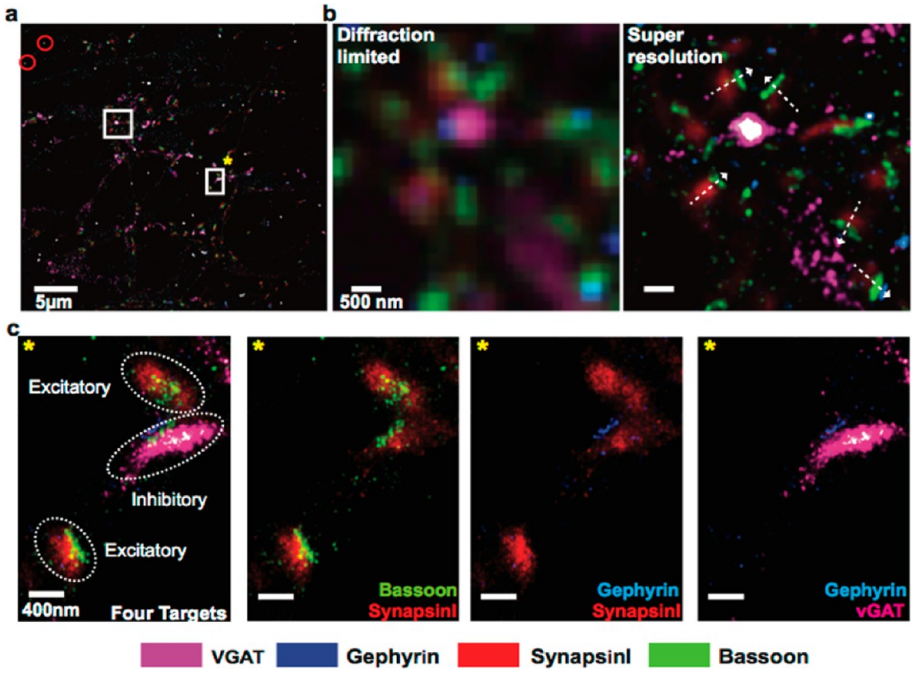

Figure 6. Co-localization of synaptic proteins detected using multiplexed Exchange-PAINT imaging. (a) The images of synaptic proteins from Figure 5 were merged using gold nanoparticles as registration markers (highlighted with red circles). Scale bar: 5 μm. (b) Comparison of diffraction-limited and super-resolution images of four synaptic proteins from the region highlighted with a white square without *. The orientation of synapses could be visualized in the super-resolved image as indicated by the white dashed arrows. Scale bar: 500 nm. (c) One region from panel a was selected for a magnified view (highlighted with a white square with *). Scale bars: 400 nm.

SynapsinI and Bassoon signals, suggesting they were excitatory synapses, whereas the middle synapse contained all four targets, indicating that it was an inhibitory synapse (Figure 6c). SynapsinI, Bassoon, and vGAT were present in the presynaptic site and therefore well-separated from the signal from Gephyrin that existed in the postsynaptic site. The distribution patterns of SynapsinI and vGAT, both of which were localized on synaptic vesicles, correlated well with each other. The result indicates Exchange-PAINT is well-suited for high-resolution visualization of protein−protein colocalization in situ.

An increasing body of effort has been devoted to molecular heterogeneity mapping in single cells. Such in situ "omics" studies, including transcriptomics and proteomics, have the potential to greatly expand our knowledge about how cells and tissues are organized to realize their biological functions. Several techniques, such as laser capture microdissection-assisted single-cell RNA sequencing,[30] Fluorescence in situ RNA sequencing,[31] highly multiplexed FISH,[32] has been developed to enable spatially resolved transcriptomics. In situ proteomics analysis, on the other hand, has not been widely performed mainly due to the lack of efficient and practical methods, particularly as existing sequential IF imaging methods require multirounds of time-intensive immunostaining. DEI herein provides a simple, efficient, and versatile tool to map diverse proteins in situ with flexible choice regarding achievable spatial resolution. It has multiple advantages: (1) DEI allows fast multiplexed data acquisition and probe exchange, as targets are simultaneously immunostained and transient binding of imagers to docking strands is rapid (minutes); (2) DEI—as other sequential imaging approaches−allows image acquisition with a single laser line, thus avoiding chromatic aberration (Figure S10) and eliminating time-consuming optimization of imaging setting (e.g., immersion medium for SIM) for individual laser channels; (3) DEI allows straightforward reimaging of earlier targets. This allows users to rapidly scan a sample e.g. using fast Exchange-Confocal to determine regions of interest and then reprobe these with shorter imager strands for higher resolution imaging, for example, using Exchange-PAINT; (4) DEI does not require specialized instruments (e.g., mass spectrometers for MIBI) or harsh buffer treatment (e.g., acidified $KMnO_4$ or H_2O_2) to quench fluorescence signals. The labeling protocols and imaging instruments are identical to standard and well-established immunostaining methods, the only difference being the use of a DNA-tagged antibody as opposed to a dye-tagged antibody, thus making it easily accessible to common biological laboratories.

A key requirement for sequential imaging is to minimize sample drift during an experiment. All of our buffer exchange experiments were performed without removing samples from the microscope stage. A fluidic chamber system has been described in our original Exchange-PAINT paper[17] and can be used to reduce the physical disturbance caused by buffer exchange. A registration marker channel, either bright field or other fluorescence channels, is required to record sample drift for postexperiment image registration. In this current study, we adapted a subpixel registration algorithm[28] that can perform translation drift correction with a user-defined up-sampling factor. It increased the registration accuracy, which is important when super-resolution imaging is performed. *Z*-axis drift can be easily managed by using commercially available focus maintaining systems.

We note that we occasionally observe nonspecific nuclear staining from DNA-conjugated primary antibodies, which is likely an antibody-specific phenomenon. Interestingly, we did not observe a similar phenomenon for DNA-conjugated secondary antibodies (Figure S11). It has been suggested that the addition of dextran sulfate to the incubation buffer can

DOI: 10.1021/acs.nanolett.7b02716
Nano Lett. 2017, 17, 6131−6139

alleviate the nonspecific binding.[33] The addition of Herring sperm DNA and polyT DNA has also been used to block nonspecific interaction caused by DNA.[14] We also notice that using saponin instead of Triton or Tween as detergent during staining does not permeabilize the nucleus membrane and hence prevents antibodies from entering the nucleus.

In summary, we have developed DNA-Exchange-Imaging as a rapid and versatile multiplexed imaging technique for both diffraction-limited and super-resolution in situ imaging in cells and in tissues. The intrinsic programmability of imager/docking strand interaction renders DEI easily adaptable to diverse imaging platforms, including standard resolution Exchange-Confocal demonstrated here, and various super-resolution methods including Exchange-SIM demonstrated here, Exchange-STED demonstrated here and in related work,[29] Exchange-STORM demonstrated in our recent related work using stably attached imager strands,[34] and Exchange-PAINT[17] demonstrated in our original work with increasing resolution. We further compared these three binding schemes (i.e., transient, semitransient, and stable binding) in Figures S2, S12, and S13, and list their pros, cons, and suitable application in Table S12. In short, the transient binding scheme enables easy DNA strand exchange but gives weak signals under the same imaging setting. In contrast, the stable binding scheme gives strong signals but requires harsher strand removal methods (i.e., formamide-containing solution). The semitransient binding retains the feature of easy DNA strand exchange and gives medium-level signals. In addition, the transient-binding scheme is suitable for DNA-PAINT super-resolution imaging. Meanwhile, the semitransient binding and stable binding schemes enable highly multiplexed confocal, SIM, STED imaging. The stable binding scheme also allows STORM imaging. Finally, the signals from both transient binding and semitransient binding schemes are tunable based on imager strand concentration and resistant to photobleaching because of replenishment of imager strands from the solution. One concern for semitransient binding compared to stable binding is that the excessive imager strands in the solution could contribute to the background and hence reduce image quality. We found that image processing (e.g., deconvolution) can be used to address the background issue and improve image quality (Figure S14). This will serve a guideline for users to choose the binding scheme based on their experiments.

Beyond these validated imaging platforms, we also expect that DEI is compatible with many other imaging methods. For example, a combination of DEI with ultrathin sectioning of samples could allow correlative light and electron microscopy imaging. Additionally, DEI is also in principle compatible with DNA mediated in situ signal amplification methods (e.g., hybridization chain reaction,[35] and rolling circle amplification[36]), potentially permitting rapid, spectrally unlimited multiplexing for low abundance targets. Combination of DEI with tissue clearing methods, such as CLARITY[37] and SWITCH,[38] would allow the imaging of a thick tissue sample. The combination of DEI with expansion microscopy[33] would further allow imaging thick samples with nanoscopic resolution. The integration of DEI with neuron tracing techniques, such as Brainbow,[39] could allow simultaneous detection of neuronal connectivity and underlying molecular characteristics, such as cell identity. The resultant "Molecular Connectome" would complement the "Anatomical Connectome"[40] and help us understand brain function across multiple scales from circuits to molecules.

■ ASSOCIATED CONTENT

Supporting Information

The Supporting Information is available free of charge on the ACS Publications website at DOI: 10.1021/acs.nanolett.7b02716.

(1) Methods (cell culture and tissue samples preparation and staining; imaging setup and acquisition; imaging analysis); (2) Supplementary Figures 1−14 (photobleaching resistance; comparison of DNA labeling schemes; exchange-STED); (3) Supplementary Tables 1−12 (comparison of DNA labeling schemes; comparison of multiplexed imaging methods; lists of DNA sequences; lists of antibodies) (PDF)

(1) 3D views of multi-targets in fixed mouse hippocampal neuron cultures. A movie was created using Imaris for 3D slicing views of the targets shown in Figure 2. Mouse hippocampal neurons were fixed using PFA and stained to target SynapsinI, vGAT, MAP2, pNFH, AlphaTubulin, AcetylTubulin, GFAP, and DAPI (AVI)

■ AUTHOR INFORMATION

Corresponding Authors

*E-mail: (P.Y.) py@hms.harvard.edu; 617-432-7731.
*E-mail: (R.J.) jungmann@biochem.mpg.de.
*E-mail: (S.S.A.) sagasti@jncasr.ac.in.

ORCID

Ralf Jungmann: 0000-0003-4607-3312
Peng Yin: 0000-0002-2769-6357

Present Addresses

S.S.A.: New Chemistry Unit and Chemistry & Physics of Materials Unit, Jawaharlal Nehru Centre for Advanced Scientific Research (JNCASR), Bangalore, India.
J.B.W., R.J.: Department of Physics and Center for Nanoscience, Ludwig Maximilian University, 80539 Munich, Germany, Max Planck Institute of Biochemistry, 802152 Martinsried near Munich, Germany.

Notes

The authors declare the following competing financial interest(s): P.Y., R.J., S.A.A., and Y.W. have filed a patent application for the reported technology. P.Y. and R.J. are cofounders of Ultivue, Inc., a startup with interests in commercializing DNA-Exchange-Imaging technology. P.Y. is also a cofounder of NuProbe Global. G.M.C. is a cofounder of ReadCoor, Inc.. E.S.B. is a cofounder of Expansion Technologies, Inc.

■ ACKNOWLEDGMENTS

We thank X. Chen, F. Schueder, and C. Cepko for helpful discussions. We thank Z. Liang for kindly providing experimental materials. We thank L. Ding from Enhanced Neuroimaging Core in Harvard for assistance in STED microscopy. This work is supported by NIH grants (1U01MH106011, 1R01EB018659), NSF grant (CCF-1317291), and ONR grants (N00014-13-1-0593 and N00014-14-1-0610) to P.Y.; Emmy Noether Fellowship (DFG JU 2957/1-1), ERC Starting Grant (MolMap, Grant agreement number 680241) and support from Max Planck Society to R.J.; Wellcome Trust-DBT India Alliance Intermediate Fellowship (IA/I/16/1/502368) to S.S.A.; NIH grant (RM1HG008525) to G.M.C.; NIH grant (R01NS083898) to P.S.K.; NIH grant (P01 CA080111.) to J.S.B.; NIH grants (1R24MH106075,

DOI: 10.1021/acs.nanolett.7b02716
Nano Lett. 2017, 17, 6131−6139

NIH 1R01NS087950, and NIH 1R01MH103910), and support from HHMI-Simons Faculty Scholars Program, the Open Philanthropy project, the MIT Media Lab, and the New York Stem Cell Foundation to E.S.B.. Y.W. acknowledges support from the Chinese Scholarship Council. M.S.A. and M.D. acknowledge support from HHMI International Student Research Fellowships. S.S.H.W. acknowledges support from NSF fellowship DGE1144152. P.W.T. acknowledges support from the Hertz Foundation.

REFERENCES

(1) Friedenberger, M.; Bode, M.; Krusche, A.; Schubert, W. *Nat. Protoc.* **2007**, *2* (9), 2285−94.
(2) Gerdes, M. J.; Sevinsky, C. J.; Sood, A.; Adak, S.; Bello, M. O.; Bordwell, A.; Can, A.; Corwin, A.; Dinn, S.; Filkins, R. J.; Hollman, D.; Kamath, V.; Kaanumalle, S.; Kenny, K.; Larsen, M.; Lazare, M.; Li, Q.; Lowes, C.; McCulloch, C. C.; McDonough, E.; Montalto, M. C.; Pang, Z.; Rittscher, J.; Santamaria-Pang, A.; Sarachan, B. D.; Seel, M. L.; Seppo, A.; Shaikh, K.; Sui, Y.; Zhang, J.; Ginty, F. *Proc. Natl. Acad. Sci. U. S. A.* **2013**, *110* (29), 11982−7.
(3) Glass, G.; Papin, J. A.; Mandell, J. W. *J. Histochem. Cytochem.* **2009**, *57* (10), 899−905.
(4) Lin, J. R.; Fallahi-Sichani, M.; Sorger, P. K. *Nat. Commun.* **2015**, *6*, 8390.
(5) Micheva, K. D.; Smith, S. J. *Neuron* **2007**, *55* (1), 25−36.
(6) Pirici, D.; Mogoanta, L.; Kumar-Singh, S.; Pirici, I.; Margaritescu, C.; Simionescu, C.; Stanescu, R. *J. Histochem. Cytochem.* **2009**, *57* (6), 567−75.
(7) Schubert, W.; Bonnekoh, B.; Pommer, A. J.; Philipsen, L.; Bockelmann, R.; Malykh, Y.; Gollnick, H.; Friedenberger, M.; Bode, M.; Dress, A. W. *Nat. Biotechnol.* **2006**, *24* (10), 1270−8.
(8) Tam, J.; Cordier, G. A.; Borbely, J. S.; Sandoval Alvarez, A.; Lakadamyali, M. *PLoS One* **2014**, *9* (7), e101772.
(9) Angelo, M.; Bendall, S. C.; Finck, R.; Hale, M. B.; Hitzman, C.; Borowsky, A. D.; Levenson, R. M.; Lowe, J. B.; Liu, S. D.; Zhao, S.; Natkunam, Y.; Nolan, G. P. *Nat. Med.* **2014**, *20* (4), 436−42.
(10) Giesen, C.; Wang, H. A.; Schapiro, D.; Zivanovic, N.; Jacobs, A.; Hattendorf, B.; Schuffler, P. J.; Grolimund, D.; Buhmann, J. M.; Brandt, S.; Varga, Z.; Wild, P. J.; Gunther, D.; Bodenmiller, B. *Nat. Methods* **2014**, *11* (4), 417−22.
(11) Levenson, R. M.; Borowsky, A. D.; Angelo, M. *Lab. Invest.* **2015**, *95* (4), 397−405.
(12) Zhang, Z.; Kenny, S. J.; Hauser, M.; Li, W.; Xu, K. *Nat. Methods* **2015**, *12* (10), 935−8.
(13) Duose, D. Y.; Schweller, R. M.; Hittelman, W. N.; Diehl, M. R. *Bioconjugate Chem.* **2010**, *21* (12), 2327−31.
(14) Schweller, R. M.; Zimak, J.; Duose, D. Y.; Qutub, A. A.; Hittelman, W. N.; Diehl, M. R. *Angew. Chem., Int. Ed.* **2012**, *51* (37), 9292−6.
(15) Zimmermann, T.; Marrison, J.; Hogg, K.; O'Toole, P. *Methods Mol. Biol.* **2014**, *1075*, 129−48.
(16) Zrazhevskiy, P.; Gao, X. *Nat. Commun.* **2013**, *4*, 1619.
(17) Jungmann, R.; Avendano, M. S.; Woehrstein, J. B.; Dai, M.; Shih, W. M.; Yin, P. *Nat. Methods* **2014**, *11* (3), 313−8.
(18) Agasti, S. S.; Wang, Y.; Schueder, F.; Sukumar, A.; Jungmann, R.; Yin, P. *Chem. Sci.* **2017**, *8* (4), 3080−3091.
(19) Jungmann, R.; Steinhauer, C.; Scheible, M.; Kuzyk, A.; Tinnefeld, P.; Simmel, F. C. *Nano Lett.* **2010**, *10* (11), 4756−61.
(20) Micheva, K. D.; Busse, B.; Weiler, N. C.; O'Rourke, N.; Smith, S. J. *Neuron* **2010**, *68* (4), 639−53.
(21) Cheng, C. L.; Djajadi, H.; Molday, R. S. *Methods Mol. Biol.* **2012**, *935*, 185−99.
(22) Swaroop, A.; Kim, D.; Forrest, D. *Nat. Rev. Neurosci.* **2010**, *11* (8), 563−76.
(23) Kim, D. S.; Ross, S. E.; Trimarchi, J. M.; Aach, J.; Greenberg, M. E.; Cepko, C. L. *J. Comp. Neurol.* **2008**, *507* (5), 1795−810.
(24) Yang, H.; Standifer, K. M.; Sherry, D. M. *J. Comp. Neurol.* **2002**, *443* (3), 275−88.
(25) Zoeller, J. J.; Bronson, R. T.; Selfors, L. M.; Mills, G. B.; Brugge, J. S. *NPJ. Breast Cancer* **2017**, *3*, 18.
(26) Viegas, M. S.; Martins, T. C.; Seco, F.; do Carmo, A. *Eur. J. Histochem.* **2007**, *51* (1), 59−66.
(27) Gustafsson, M. G.; Shao, L.; Carlton, P. M.; Wang, C. J.; Golubovskaya, I. N.; Cande, W. Z.; Agard, D. A.; Sedat, J. W. *Biophys. J.* **2008**, *94* (12), 4957−70.
(28) Guizar-Sicairos, M.; Thurman, S. T.; Fienup, J. R. *Opt. Lett.* **2008**, *33* (2), 156−8.
(29) Beater, S.; Holzmeister, P.; Lalkens, B.; Tinnefeld, P. *Opt. Express* **2015**, *23* (7), 8630−8.
(30) Zeisel, A.; Munoz-Manchado, A. B.; Codeluppi, S.; Lonnerberg, P.; La Manno, G.; Jureus, A.; Marques, S.; Munguba, H.; He, L.; Betsholtz, C.; Rolny, C.; Castelo-Branco, G.; Hjerling-Leffler, J.; Linnarsson, S. *Science* **2015**, *347* (6226), 1138−42.
(31) Lee, J. H.; Daugharthy, E. R.; Scheiman, J.; Kalhor, R.; Yang, J. L.; Ferrante, T. C.; Terry, R.; Jeanty, S. S.; Li, C.; Amamoto, R.; Peters, D. T.; Turczyk, B. M.; Marblestone, A. H.; Inverso, S. A.; Bernard, A.; Mali, P.; Rios, X.; Aach, J.; Church, G. M. *Science* **2014**, *343* (6177), 1360−3.
(32) Chen, K. H.; Boettiger, A. N.; Moffitt, J. R.; Wang, S.; Zhuang, X. *Science* **2015**, *348* (6233), aaa6090.
(33) Chen, F.; Tillberg, P. W.; Boyden, E. S. *Science* **2015**, *347* (6221), 543−8.
(34) Schueder, F.; Strauss, M. T.; Hoerl, D.; Schnitzbauer, J.; Schlichthaerle, T.; Strauss, S.; Yin, P.; Harz, H.; Leonhardt, H.; Jungmann, R. *Angew. Chem., Int. Ed.* **2017**, *56* (14), 4052−4055.
(35) Dirks, R. M.; Pierce, N. A. *Proc. Natl. Acad. Sci. U. S. A.* **2004**, *101* (43), 15275−8.
(36) Schweitzer, B.; Wiltshire, S.; Lambert, J.; O'Malley, S.; Kukanskis, K.; Zhu, Z.; Kingsmore, S. F.; Lizardi, P. M.; Ward, D. C. *Proc. Natl. Acad. Sci. U. S. A.* **2000**, *97* (18), 10113−9.
(37) Chung, K.; Wallace, J.; Kim, S. Y.; Kalyanasundaram, S.; Andalman, A. S.; Davidson, T. J.; Mirzabekov, J. J.; Zalocusky, K. A.; Mattis, J.; Denisin, A. K.; Pak, S.; Bernstein, H.; Ramakrishnan, C.; Grosenick, L.; Gradinaru, V.; Deisseroth, K. *Nature* **2013**, *497* (7449), 332−7.
(38) Murray, E.; Cho, J. H.; Goodwin, D.; Ku, T.; Swaney, J.; Kim, S. Y.; Choi, H.; Park, Y. G.; Park, J. Y.; Hubbert, A.; McCue, M.; Vassallo, S.; Bakh, N.; Frosch, M. P.; Wedeen, V. J.; Seung, H. S.; Chung, K. *Cell* **2015**, *163* (6), 1500−14.
(39) Cai, D.; Cohen, K. B.; Luo, T.; Lichtman, J. W.; Sanes, J. R. *Nat. Methods* **2013**, *10* (6), 540−7.
(40) Lichtman, J. W.; Pfister, H.; Shavit, N. *Nat. Neurosci.* **2014**, *17* (11), 1448−54.

DOI: 10.1021/acs.nanolett.7b02716
Nano Lett. 2017, 17, 6131−6139